IOP Conference Series: Earth and Environmental Science

**PAPER** • **OPEN ACCESS**

# Interannual and Seasonal Cycles of $CO_2$ from GOSAT and AIRS

To cite this article: N Ying *et al* 2019 *IOP Conf. Ser.: Earth Environ. Sci.* **237** 022003

View the article online for updates and enhancements.

This content was downloaded from IP address 218.22.7.62 on 08/11/2019 at 12:48

# Interannual and Seasonal Cycles of $CO_2$ from GOSAT and AIRS

**N YING [1], Q YE [1], J J XIA[2]**

[1]Faculty of Geographical Science, Beijing Normal University, Beijing 100875, China

[2]Institute of Atmospheric Physics, Chinese Academy of Sciences, Beijing 100029, China

[*]Corresponding author's e-mail: yingna@mail.bnu.edu.cn

**Abstract.** In this paper, the spatiotemporal variations of carbon dioxide ($CO_2$) are examined using the $CO_2$ datasets retrieved from the Greenhouse Gases Observing Satellite (GOSAT) and Atmospheric Infrared Sounder (AIRS). These results demonstrate that the distribution of GOSAT $CO_2$ is strongly influenced by $CO_2$ emissions from human activities and natural processes, while the characteristics of AIRS $CO_2$ are concerned with both surface sources and large-scale circulation systems. Meanwhile, the spatial difference (GOSAT minus AIRS) ranges from 2–10 ppm, with a maximum value near the Greenland region (>8 ppm). The major pattern of both GOSAT and AIRS $CO_2$ variability exhibits a gradual increase globally. The dominant pattern of GOSAT is proportional to its average distribution, while the leading distributions of AIRS are relatively mixing homogeneity. Additionally, the seasonal amplitudes of GOSAT $CO_2$ are larger in Northeast Asia and Northeast North American (>10 ppm). The largest fluctuation of AIRS $CO_2$ occurs in the Arctic zone, which is dominated by the carbon cycle of the terrestrial biosphere. The seasonal fluctuation from the column-averaged $CO_2$ is more significant than that in the mid-tropospheric $CO_2$, possibly because of tropospheric adjustments of sensible and latent heat at the tropopause. These results regarding the spatial patterns of $CO_2$ at the global scale will help us to better understand the vertical transport of $CO_2$ and its impact on climate change.

## 1.Introduction

As a result of fossil fuel emissions, the concentrations of carbon dioxide ($CO_2$) in the atmosphere have increased from 280 ppm in the pre-industrial era to 405.1 ppm in 2016 [1]. Consistently increasing $CO_2$ concentrations in the atmosphere can significantly influence the radiative forcing and surface energy balance, leading to global warming [2–3]. To better understand the impacts of $CO_2$ on climate, it is essential to clarify the distribution and variability of $CO_2$ [4].

$CO_2$ concentrations have been monitored systematically at many places around the world since the mid-1950s. Furthermore, monitoring has since expanded to a global network of ground-based flask observations [5]. However, these measurements are too sparse to obtain information on regional or global distributions of $CO_2$ concentrations. Recently, satellite observation has become an effective approach to monitoring the spatial coverage of $CO_2$ on a continuous basis. Substantial progress has also been made in understanding the spatiotemporal patterns of atmospheric $CO_2$. Utilizing the mid-tropospheric $CO_2$ data from the Atmospheric Infrared Sounder (AIRS), it has been found that the variability of AIRS $CO_2$ is influenced by both surface factors [6] as well as large-scale circulation systems, such as the Madden–Julian Oscillation [7], El Niño–Southern Oscillation [8], and South-

Content from this work may be used under the terms of the Creative Commons Attribution 3.0 licence. Any further distribution of this work must maintain attribution to the author(s) and the title of the work, journal citation and DOI.
Published under licence by IOP Publishing Ltd

Atlantic Walker circulation [9]. Additionally, important studies have also been conducted using Greenhouse Gases Observing Satellite (GOSAT) data to investigate the spatial distributions of anthropogenic emissions [10, 11] and identify net fluxes [2–3].

Presently, however, we still do not know enough about the characteristics of atmospheric $CO_2$ in terms of its interannual and seasonal variations at large continental scales. More importantly, their spatial differences remain poorly understood. In the present study, GOSAT and AIRS datasets were used to analyse the temporal characteristics of trends and variations of $CO_2$ over the globe. The primary objective of the work was to explore the temporal characteristics and correlations between column-averaged $CO_2$ concentrations and mid-tropospheric $CO_2$ changes.

## 2.DATA AND METHODS

### *2.1 $CO_2$ data*

GOSAT and AIRS data were employed to explore the spatial patterns. GOSAT was the first space-based orbiting to monitoring carbon dioxide ($CO_2$) and methane (CH4), launched in January 2009 [14–15]. $CO_2$ retrieval data (FTS SWIR Level 3 V02.26, bias corrected) are available from June 2009 to April 2014 and can be download from https://data2.gosat.nies.go.jp. The spatial resolution of GOSAT's $CO_2$ data is 2.5° latitude × 2.5° longitude.

AIRS was the first instrument to detect mid-tropospheric $CO_2$ [16–17]. AIRS (V005 Level 3 Monthly) $CO_2$ retrievals are available at a spatial resolution of 2° latitude × 2.5° longitude, from September 2002 to the present day. The data can be downloaded from https://disc.gsfc.nasa.gov/datasets/AIRS3C2M_V005/.

In this study, considering the continuous period of GOSAT, we selected the monthly-mean $CO_2$ from July 2009 to April 2014 as the study period (total of 58 months). The AIRS data were interpolated to 2.5° × 2.5°. We excluded the regions around the South Pole (60°S–90°N), which are poorly covered by the retrievals or have large retrieval errors. The Mauna Loa (MLO) station record at the same time was also selected, to compare with the AIRS and GOSAT data.

### *2.2 Methods*

To isolate the prominent patterns of $CO_2$ and their temporal variability, empirical orthogonal function (EOF) analysis has been performed [18]. We decomposed the data into EOFs, which define the spatial patterns and the accompanying principal components (PCs) characterizing the temporal behavior of these patterns. They were determined here using the singular value decomposition code available in Matlab. Prior to computing the EOFs, we removed the seasonality of the data by subtracting the calendar-month mean from each grid point, so that the calculated EOFs referred to the tendency distribution:

$$C_i^y(m) = C'^y_i(m) - \mathrm{mean}(C'^y_i(m))$$

Where $y$ indexes the year and $i$ indexes the nodes. The $CO_2$ anomaly time series, $C_i^y(m)$, is constructed by removing the seasonal cycle.

## 3.RESULTS AND DISCUSSION

### *3.1 Spatiotemporal characteristics of $CO_2$*

The time series of monthly global-mean $CO_2$ concentrations from AIRS, MLO and GOSAT is shown in figure 1. Each data source shows predominant rising trends and seasonal variations of $CO_2$. The 58-month averages of GOSAT, AIRS and MLO $CO_2$ are 389 ppm, 392 ppm and 392.3 ppm, respectively. The global mean $CO_2$ concentration retrieved from AIRS is about 3 ppm higher than that from GOSAT. As described in the GOSAT Validation Report [19], GOSAT $CO_2$ data are, on average, 1.2 ppm lower than Total Carbon Column Observing Network (TCCON) data. So, 40% of the observed bias (1.2 ppm/3 ppm) can be explained by the biases inherent to the GOSAT product.

The peak-to-trough variation amplitude of the AIRS $CO_2$ matches the MLO data, as they have the same retrieved height. The spatial distribution of GOSAT $CO_2$ has a clear north–south gradient [Fig. 1(b)]. Higher concentrations occur in East and West Asia, the Southeast U.S., Central South America, Central Africa, and West Europe. The spatial pattern of AIRS $CO_2$ is characterized by a strong contrast between the Northern Hemisphere (NH) and Southern Hemisphere (SH). In the NH, large enhancements occur over a belt from 35°N to 45°N and in the northern Polar Regions.

We further quantified the spatial pattern of the difference between the GOSAT and AIRS $CO_2$ [Fig. 1(d)]. The results show that the difference (GOSAT minus AIRS) varies from 2 to 10 ppm, and the greater discrepancy is concentrated at higher latitudes (above 60°N). More specifically, the largest difference occurs over the Arctic region (>6 ppm), especially over the Greenland region (>8 ppm). We also find that the negative values (<2 ppm) are concentrated over the northern tropical Pacific Ocean.

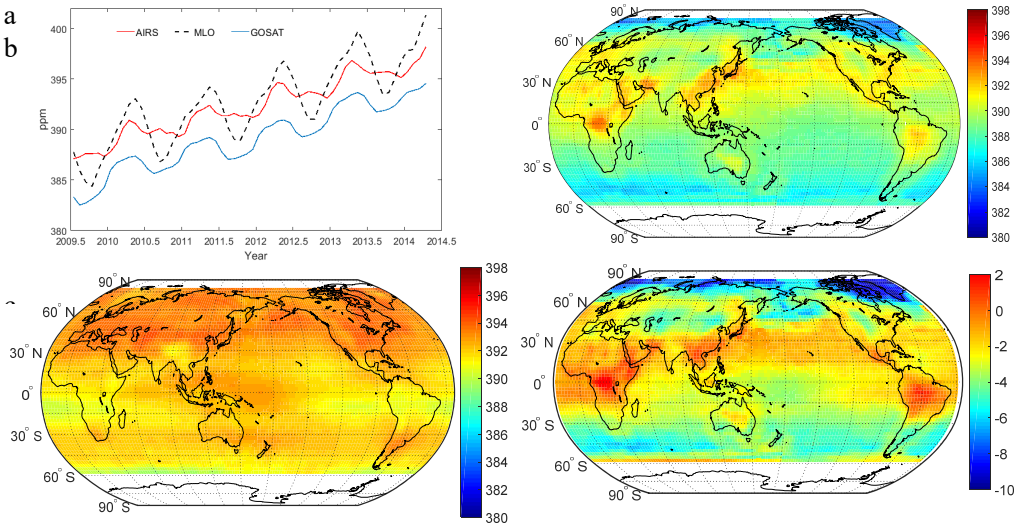



Figure 1. (a) Time–series of monthly average AIRS, MLO and GOSAT $CO_2$ concentrations for the studied period; (b) The spatial distribution of monthly mean GOSAT $CO_2$; (c) The spatial distribution of monthly mean AIRS $CO_2$; (d) Differences between AIRS $CO_2$ and GOSAT $CO_2$ (AIRS minus GOSAT). Units: ppm

### *3.2 Methods Interannual variations of $CO_2$*

The first mode of deseasonlized GOSAT and AIRS $CO_2$ explains 90.3% and 85.3% of the variability [Table 1]. The EOF-1 of the GOSAT $CO_2$, shown in Fig. 2(a), displays a global increase, with maximum values over land regions. The EOF-1 of the AIRS $CO_2$ [Fig. 2(b)] exhibits a global rising mode, with significant enhancement over the Middle East and the Mediterranean. The second EOF (2.68% of the variability) of GOSAT displays opposite polarity between the Arctic region and southern regions [Fig. 2(c)]. The EOF-2 of AIRS [Fig. 2(d)] is similar to that of GOSAT, with a large area in North Asia. The PCs corresponding to EOF-1 are separately shown in Fig. 2(e). The PC-1 time series is remarkably linear in their increase, and oscillates with annual periodicities. The PC-2 displays semi-annual and annual variability.

Table 1. Variances (in %) accounted for by the first five PCs of the AIRS and GOSAT $CO_2$.

| **$CO_2$** | **λ1** | **λ2** | **λ3** | **λ4** | **λ5** |
|---|---|---|---|---|---|
| GOSAT | 90.3% | 2.68% | 0.94% | 0.66% | 0.51% |
| AIRS | 85.3% | 3.3% | 2.08% | 1.06% | 0.98% |

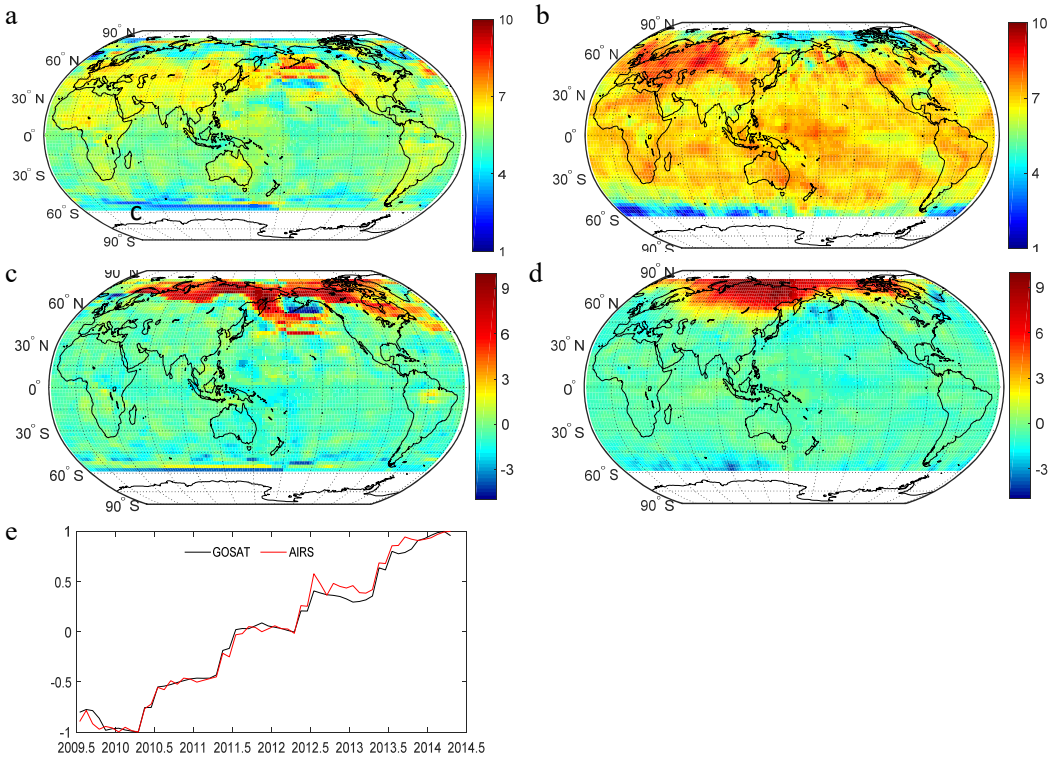



Figure 2. The $CO_2$ EOFs and the corresponding normalized PCs of the $CO_2$ (in ppm). The first modes of GOSAT $CO_2$ (a) and AIRS $CO_2$ (b); the second modes of GOSAT $CO_2$ (c) and AIRS $CO_2$ (d). The normalized PC– 1(e) and PC–2 (f) of the GOSAT and AIRS $CO_2$.

### *3.3 Seasonal variations of $CO_2$*

The difference between the maximum and minimum months of monthly $CO_2$ is utilized to explain the amplitude of the seasonal cycle. The long-term increasing trend was removed before calculation of the difference between the maximum and minimum concentrations in a year. Although the global average peaks in April, regional differences still exist. The seasonal amplitude of the GOSAT $CO_2$ is shown in Fig. 3(a). In the NH, a larger $CO_2$ seasonal amplitude can be clearly seen over northeast Asia (>12 ppm), northeast North America (>10 ppm), and the northern tropical Pacific Ocean (>6 ppm). Conversely, in the SH tropics, we see significantly lower levels of $CO_2$, with lower seasonal variability that correlates well with tropical rainforest regions.

Figure 3(b) shows the seasonal amplitude of the AIRS $CO_2$. Higher variations are observed in the transition zone across the Aleutian Islands and Alaskan Gyre (≥8 ppm). The transition region witnesses these seasonal variations with a maximum and minimum in April and November, respectively. This region is a large sink for atmospheric $CO_2$, where $CO_2$ uptake dominates from April through November. Moreover, we also see a large enhancement over the Greenland region (≥12 ppm). It can be discerned that the seasonal signals of $CO_2$ reach a maximum in April and minimum in July. The seasonal amplitude of AIRS shows similar results to GOSAT in the SH. In the NH, the GOSAT measurements exhibit strong amplitude, due to their sensitivity to the near-surface $CO_2$, where the impact of the seasonal summer uptake by vegetation and the ocean sink are more pronounced [20].

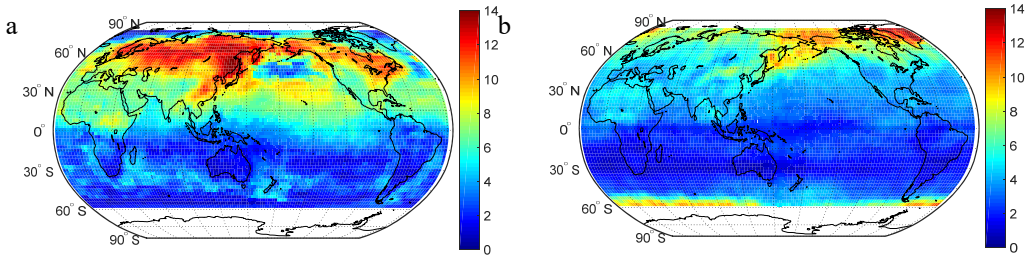



Figure 3. The distribution of seasonal fluctuations of GOSAT(a) and AIRS(b) retrieved $CO_2$ (in ppm)

## 4.CONCLUSION

In this study, we analysed the temporal and spatial variations of satellite-derived, column-averaged and mid-tropospheric $CO_2$, and associated the observed variability with known atmospheric transport processes, as well as sources and sinks of $CO_2$.

The GOSAT $CO_2$ data and AIRS mid-tropospheric $CO_2$ data show consistency with the MLO observations. We have shown that the distribution of the GOSAT $CO_2$ is strongly influenced by $CO_2$ emissions from human activities and natural processes. The characteristics of the AIRS $CO_2$ are related to both surface sources and large-scale circulation systems [21–22], such as convection and eddy mixing. The monthly average bias between GOSAT and AIRS is 3 ppm, while their spatial difference (GOSAT minus AIRS) ranges from 2–10 ppm. The distribution suggests a dominant transport pathway for lifting pollution from the column average (GOSAT) into the middle and upper troposphere [23]. The dominant modes of the GOSAT and AIRS $CO_2$ explain 90.3% and 85.3% of the variability, respectively. The leading pattern from GOSAT displays a global increase over land regions, while the AIRS pattern exhibits a relatively homogeneous rising mode.

Additionally, the distribution of seasonal amplitudes was also analysed. The significant GOSAT $CO_2$ seasonal amplitudes were found to occur in northeast Asia, northeast North America, and over the northern tropical Pacific Ocean. The distributions are dominated by the carbon cycle of the terrestrial biosphere [24] and the long-range transport of pollutants from Asia to the Asian Pacific region [25]. Moreover, the centre of the AIRS seasonal variations is located in the transition zone across the Aleutian Islands and Alaskan Gyre ($\geq$ 8ppm) and Greenland region ($\geq$ 12 ppm). The seasonal variations present significant differences in the Arctic regions, indicating the function of tropospheric adjustments of sensible and latent heat at the tropopause [26].

Lastly, it is important to note that, since no 3-D transport model was used in this study, the origins of the $CO_2$ concentrations and the feedback of the spatial distribution of $CO_2$ to climate change need further and more detailed study.

**Acknowledgments**

This work was supported by the National Key Research and Development Program of China (Grant No. 2016YFA0602503). We thank the members of the GOSAT Project for providing the GOSAT Level 3 data products, and NASA for providing the AIRS $CO_2$ datasets.

**References**

[1] World Meteorological Organization, WMO Greenhouse Gas Bulletin No.13, 2016. The State of Greenhouse Gases in the Atmosphere Based on Global Observations through. http://www.wmo.int/pages/prog/arep/gaw/ghg/GHGbulletin.html.

[2] Stocker, T.F., Qin, D., Plattner, G.K., Tignor, M., Allen, S.K., Boschung, J., Midgley, P.M. (2013) Contribution of working group I to the fifth assessment report of the intergovernmental panel on climate change. Climate change 2013: the physical science basis: 1535–1535

[3] Feldman, D.R., Collins, W.D., Gero, P.J., Torn, M.S., Mlawer, E.J., Shippert, T.R. (2015) Observational determination of surface radiative forcing by $CO_2$ from 2000 to 2010. Nature, 519: 339–343.

[4] Keeling, C.D., J. A.A. Jr, C. A.E. Jr, Guenther, P.R. (1976) Atmospheric $CO_2$ variations at the South Pole. Tellus, 28: 552–564.
[5] Cooperative Global Atmospheric Data Integration Project. 2013, updated annually. Multi-laboratory compilation of synchronized and gap-filled atmospheric carbon dioxide records for the period 1979-2012 (obspack_co2_1_GLOBALVIEW-CO2_2013_v1.0.4_2013-12-23). Compiled by NOAA Global Monitoring Division: Boulder, Colorado, U.S.A. Data product accessed at http://dx.doi.org/10.3334/OBSPACK/1002
[6] Pagano, T.S., Olsen, E.T., Nguyen, H., Ruzmaikin, A., Jiang, X., Perkins, L. (2014) Global variability of midtropospheric carbon dioxide as measured by the atmospheric infrared sounder. J. Appl. Remote Sens., 8: 4480–4494.
[7] Li, K.F., Tian, B., Waliser, D.E., Yung, Y.L. (2010) Tropical mid–tropospheric $CO_2$ variability driven by the Madden–Julian Oscillation. Proc. Nat. Acad. Sci. USA, 107: 19171–19175.
[8] Jiang, X., Chahine, M.T., Olsen, E.T., Chen, L.L., Yung, Y.L. (2010) Interannual variability of mid–tropospheric $CO_2$ from Atmospheric Infrared Sounder. Geophys. Res. Lett., 37: L13801– L13801.
[9] Jiang, X., Olsen, E.T., Pagano, T.S., Su, H., Yung, Y.L. (2015) Modulation of midtropospheric $CO_2$ by the South Atlantic Walker Circulation. J. Atmos. Sci., 72: 2241–2247.
[10] Kort, E.A., Frankenberg, C., Miller, C.E., Oda, T. (2012) Space–based observations of megacity carbon dioxide. Geophys. Res. Lett., 39: 17806–17806.
[11] Keppel–Aleks, G., Wennberg, P.O., O'Dell, C.W., Wunch, D. (2013) Towards constraints on fossil fuel emissions from total column carbon dioxide. Atmos. Chem. Phys., 13: 4349–4357.
[12] Basu, S., Guerlet, S., Butz, A., Houweling, S., Hasekamp, O., Aben, I. (2013) Global $CO_2$ fluxes estimated from GOAST retrievals of total column $CO_2$. Atmos. Chem. Phys., 13: 8695–8717.
[13] Maksyutov, S., Takagi, H., Kim, H., Zhuravlev, R., Saeki, T., Belikov, D. (2013) Regional $CO_2$ flux estimates for 2009–2010 based on GOSAT and ground–based $CO_2$ observations. Atmos. Chem. Phys., 12: 29235–29288.
[14] Yokota, T., Yoshida, Y., Eguchi, N., Ota, Y., Tanaka, T., Watanabe, H., Maksyutov, S. (2009) Global concentrations of $CO_2$ and $CH_4$ retrieved from GOSAT: First preliminary results. SOLA, 5: 160–163.
[15] Kuze, A., Suto, H., Nakajima, M., Hamazaki, T. (2009) Thermal and near infrared sensor for carbon observation fourier–transform spectrometer on the greenhouse gases observing satellite for greenhouse gases monitoring. Appl. Opt., 48: 6716–6733.
[16] Chahine, M.T., Chen, L., Dimotakis, P., Jiang, X., Li, Q., Olsen, E.T., Yung, Y.L. (2008) Satellite remote sounding of mid–tropospheric $CO_2$. Geophys. Res. Lett., 35: 179–190.
[17] Chahine, M., Barnet, C., Olsen, E.T., Chen, L., Maddy, E. (2005) On the determination of atmospheric minor gases by the method of vanishing partial derivatives with application to $CO_2$. Geophys. Res. Lett., 32: 154–164.
[18] Lian, T., Chen, D. (2012) An evaluation of rotated EOF analysis and its application to tropical Pacific SST variability. J. Clim., 25(15): 5361–5373.
[19] NIES GOSAT Project (2012) Summary of GOSAT Level 2 Data Product Validation Activity. https://data2.gosat.nies.go.jp/doc/documents ValidationResult_FTSSWIRL2_V02.xx_GU_en.pdf
[20] Lindqvist, H., O'Dell, C., Basu, S., Boesch, H., Chevallier, F., Deutscher, N. (2015) Does GOAST capture the true seasonal cycle of carbon dioxide? Atmo. Chem. Phys., 15: 16461–16503.
[21] Stohl, A., Eckhardt, S., Forster, C., James, P., Spichtinger, N. (2002) On the pathways and timescales of intercontinental air pollution transport. J. Geophys. Res., 107: 4684–4684.
[22] Zhang, L., Jacob, D.J., Bowman, K.W., Logan, J.A., Solène Turquety, Hudman, R.C. (2006) Ozone–co correlations determined by the tes satellite instrument in continental outflow regions. Geophys. Res. Lett., 33: L18804– L18804.

[23] Shia, R.L., Liang, M.C., Miller, C.E., Yung, Y.L. (2006) $CO_2$ in the upper troposphere: influence of stratosphere–troposphere exchange. Geophys. Res. Lett., 33: 289–289.
[24] Shim, C., Lee, J., Wang, Y. (2013) Effect of continental sources and sinks on the seasonal and latitudinal gradient of atmospheric carbon dioxide over East Asia. Atmos. Environ., 79: 853–860.
[25] Liang, Q., Jaeglé, L., Jaffe, D.A., Weiss–Penzias, P., Heckman, A., Snow, J.A. (2004) Long–range transport of Asian pollution to the northeast Pacific: Seasonal variations and transport pathways of carbon monoxide. J. Geophys. Res. Atmos., 109: 1–18.
[26] Shia, R.L., Liang, M.C., Miller, C.E., Yung, Y.L. (2006) $CO_2$ in the upper troposphere: Influence of stratosphere–troposphere exchange. Geophys. Res. Lett., 33: 289–289.